INTERNATIONAL JOURNAL FOR NUMERICAL METHODS IN ENGINEERING

Int. J. Numer. Meth. Engng 2010; **00**:1–32 *Prepared using* nmeauth.cls *[Version: 2000/01/19 v2.0]*

Harmonic enrichment functions: A unified treatment of multiple, intersecting and branched cracks in the extended finite element method

S. E. Mousavi[1] and E. Grinspun[2] and N. Sukumar[1,*]

[1] *Department of Civil and Environmental Engineering, University of California, Davis, CA 95616, USA*

[2] *Department of Computer Science, Columbia University, New York, NY 10027, USA*

SUMMARY

A unifying procedure to numerically compute enrichment functions for elastic fracture problems with the extended finite element method is presented. Within each element that is intersected by a crack, the enrichment function for the crack is obtained via the solution of the Laplace equation with Dirichlet and vanishing Neumann boundary conditions. A single algorithm emanates for the enrichment field for multiple cracks as well as intersecting and branched cracks, without recourse to special cases, which provides flexibility over existing approaches in which each case is treated separately. Numerical integration is rendered to be simple—there is no need for partitioning of the finite elements into conforming subdivisions for the integration of discontinuous or weakly singular kernels. Stress intensity factor computations for different crack configurations are presented to demonstrate the accuracy and versatility of the proposed technique.

*Correspondence to: N. Sukumar, Department of Civil and Environmental Engineering, University of California, Davis, CA 95616. E-mail: nsukumar@ucdavis.edu

KEY WORDS: partition of unity method (PUM), extended finite element method (X-FEM), harmonic enrichment, intersecting crack, branched crack, curved crack, stress intensity factors

1. INTRODUCTION

In the extended finite element method (X-FEM) [1, 2], crack modeling is performed by enriching the finite element approximation through the framework of partition of unity [3, 4]. To represent the crack, the near-tip asymptotic functions and a discontinuous function are used as enrichment functions, and fracture simulations for different crack configurations are carried out on a fixed finite element mesh. Closely-related approaches to modeling discontinuities within the partition-of-unity framework include the manifold method [5–7], the finite cover method [8], and the method of Hansbo and Hansbo [9]. In this paper, we adopt *harmonic enrichment functions* [10] to describe cracks in the extended finite element method. The approach herein unifies the procedure for crack modeling in the X-FEM with two distinct advantages: (1) numerically computed enrichment functions are constructed for cracks that naturally generalizes for the treatment of multiple cracks as well as intersecting and branched cracks. This provides flexibility over existing approaches [11–14], where each case is handled separately and the number of cases and the associated combinatorics quickly becomes unfavorable when complex patterns of multiple cracks and branches are present inside an element; and (2) partitioning of the finite elements is not required to compute the stiffness matrix.

Recently, with an eye on graphics simulations, Kaufmann et al. [10] conceived a new enrichment strategy to represent highly detailed, complex cuts through coarse elements. They

showed that a generalized harmonic enrichment function, which is the numerical solution to the Laplace equation with Dirichlet and Neumann boundary conditions, can serve as a suitable enrichment function for the entire crack discontinuity. Since the discontinuous near-tip function [1] and the generalized Heaviside function [2] are harmonic, the Laplace equation recovers both. The use of numerical harmonic enrichment functions departs from previous fracture studies on the extended finite element method where analytical enrichment functions are used: arbitrary branched and intersecting cracks [11, 12, 15], cracks in Mindlin-Reissner plates [16], polycrystals with discontinuous grain boundaries [13], bimaterial interface cracks [17], cracks in orthotropic media [18], cracks in piezoelectric materials [19], cohesive cracks [20, 21], and elastic-plastic fracture in power-law hardening materials [22] to name a few applications. In fracture computations, use of numerically computed enrichment functions has been limited. Strouboulis et al. [23, 24] construct enrichment functions for square voids and bifurcated cracks—that do not admit analytical solutions—by solving auxiliary canonical boundary-value problems. Duarte and Kim [25] adopt a global-local approach to build numerical enrichment functions tailored for three-dimensional fracture analyses. First, the global problem is solved over a coarse mesh and the solution is applied as the boundary conditions for a local problem that is specifically designed for local features of interest. Then, the solution of the local problem is used as the enrichment for the global problem.

For multiple cracks, and intersecting and branched cracks in the X-FEM, determining whether or not a specific type of enrichment function is present and the criteria for selecting the enriched nodes tends to be cumbersome. Daux et al. [11] treat branched and intersecting cracks as a main crack and consider each of the branches as separate cracks. Distinct types of enrichment functions for the crack-tip, crack interior, and the junction are used. For the

main and branch cracks, Heaviside and near-tip enrichments are adopted. Furthermore, an additional (junction) enrichment is required to model the point where the cracks meet. The junction enrichment assumes the values of -1, 0 and 1 in the three regions around the junction-point. This enrichment strategy is problem-dependent. On adopting the algorithm proposed in Reference [13], Duarte et al. [14] use a discontinuous function that is unity within a domain in the neighborhood of a branched crack and zero elsewhere to model a branched crack. This technique simplifies the enrichment strategy, but it remains problem-dependent: selection of the regions where the branch enrichment functions take on a non-zero value, depends on how the cracks interact. Furthermore, as in the standard X-FEM [2], inclusion of discontinuous functions in the trial space requires partitioning of the finite elements for the computation of element stiffness matrices, which complicates the implementation for intersecting and branched cracks.

In this paper, we adopt the technique of Kaufmann et al. [10] to compute harmonic enrichment functions, and use it for crack modeling and stress intensity factor (SIF) computations within the X-FEM. The domain of the Laplace equation (hereon referred to as the Laplace domain) is the union of all the finite elements that are enriched for any of the cracks. This domain is further discretized into a regular subgrid mesh and the finite element stiffness matrix of the Laplace equation is set up and solved over the subgrid to obtain the harmonic enrichment function. In Kaufmann et al. [10], the crack has finite width—that of a subgrid element. Though suitable for computer graphics applications, this smearing of the crack can not capture the physics of a strong discontinuity. To resolve this issue and yet retain algorithmic simplicity, we approximate the crack by a staircase path that passes along the edges of the subgrid element without intersecting its interior—a *rasterized* (Manhattan path)

description of the crack geometry emanates. In the Laplace solve, the enrichment function for each crack is obtained by imposing Dirichlet boundary conditions along the rasterized crack path ($+1$ and -1 values are imposed on duplicated nodes that lie on the crack path; 0 values are imposed on the crack-tips) of the subgrid mesh, and vanishing Neumann boundary conditions along all other cracks and boundaries. We point out that our technique is distinct from the global-local approach of Duarte and Kim [25]—in our approach the local solution for the enrichment function is independent of the global problem and is solved separately.

In the standard X-FEM, the stiffness matrix of enriched elements requires the integration of discontinuous and weakly singular functions. The numerical integration is performed by partitioning the finite elements into conforming subdivisions and using standard Gauss quadrature over these partitions [2]. More sophisticated schemes such as integration of equivalent polynomials [26], quadratures with variable weights [27], and generalized Gaussian quadrature rules with polynomial-precision over arbitrary polygons [28, 29] have also been proposed. Integration of weakly singular kernels can be carried out in one of several ways: with higher-order Gauss quadrature over the partitions [2], using adaptive integration schemes [30], or through different types of singular mappings [29, 31–33]. For a more complete list of numerical integration schemes used for the integration of discontinuous and singular functions, see References [29, 34] and the references therein. In our algorithm, the Laplace domain is discretized with conforming subgrid elements—the subgrid mesh is nested within the coarse finite element mesh. Since the harmonic enrichment function is a bilinear polynomial over each subgrid element, numerical integration on the subgrid mesh provides exact integration of the weak form integrals. Therefore, a uniform procedure emerges for the numerical integration over enriched elements, which is independent of the enrichment type or crack geometry.

The discretization of the Laplace domain without the use of such a nested subgrid mesh is undesirable, since it would produce derivative-discontinuities of the basis functions within the subgrid elements, which would preclude exact numerical integration.

We begin with the presentation of the weak form of the governing equations and a brief introduction to the extended finite element approximation (Section 2), laying the groundwork for the use of harmonic enrichment functions, which are numerically computed (Section 3). Convergence of the extended finite element method with harmonic enrichment functions is studied in Section 4. We demonstrate the accuracy and versatility of the approach with numerous benchmark crack problems (Section 5). The main findings from this work are summarized in Section 6, and we close with some final remarks.

2. EXTENDED FINITE ELEMENT METHOD

Consider the domain Ω with boundary $\Gamma = \Gamma_u \cup \Gamma_t \cup \Gamma_c$ as shown in Figure 1. The displacement boundary condition is prescribed over Γ_u and the traction is prescribed over Γ_t. The boundary Γ_c is composed of all crack faces that are assumed to be traction-free. The strong form for elastostatics is:

$$\begin{aligned} \boldsymbol{\nabla} \cdot \boldsymbol{\sigma} &= \mathbf{0} \text{ in } \Omega \\ \mathbf{u} &= \bar{\mathbf{u}} \text{ on } \Gamma_u \\ \boldsymbol{\sigma} \cdot \mathbf{n} &= \bar{\mathbf{t}} \text{ on } \Gamma_t \\ \boldsymbol{\sigma} \cdot \mathbf{n} &= \mathbf{0} \text{ on } \Gamma_c, \end{aligned} \tag{1}$$

where $\boldsymbol{\sigma}$ is the Cauchy stress tensor, $\mathbf{u}$ is the displacement, $\mathbf{n}$ is the unit outward normal and $\bar{\mathbf{u}}$ and $\bar{\mathbf{t}}$ are the prescribed displacements and tractions on Γ_u and Γ_t, respectively. On using the linear elastic constitutive law $\boldsymbol{\sigma} = \mathbf{C} : \boldsymbol{\varepsilon}$, the weak form of the boundary-value problem in (1) is: find $\mathbf{u} \in \mathcal{U}$ such that

$$\int_\Omega \boldsymbol{\varepsilon}(\mathbf{u}) : \mathbf{C} : \boldsymbol{\varepsilon}(\mathbf{v}) d\Omega = \int_{\Gamma_t} \bar{\mathbf{t}} \cdot \mathbf{v} d\Gamma \ \forall \mathbf{v} \in \mathcal{U}_0, \tag{2}$$

where $\mathcal{U}$ and $\mathcal{U}_0$ are the trial and test spaces, respectively, which are determined by the regularity of the solution ($\mathcal{U}$ and $\mathcal{U}_0$ include functions that are discontinuous across Γ_c), $\boldsymbol{\varepsilon}$ is the small-strain tensor, and $\mathbf{C}$ is the material moduli tensor. After discretizing the domain, the trial function in the extended finite element method takes the following general form [11]:

$$\begin{aligned}\mathbf{u}^h(\mathbf{x}) = &\sum_{I\in\mathcal{N}} N_I(\mathbf{x})\mathbf{u}_I + \sum_{c=1}^{n_c}\sum_{I\in\mathcal{N}_c} N_I(\mathbf{x})H_c(\mathbf{x})\mathbf{a}_{Ic} \\ &+ \sum_{t=1}^{n_t}\sum_{I\in\mathcal{N}_t}\sum_{\alpha=1}^{4} N_I(\mathbf{x})\Phi_{\alpha t}(\mathbf{x})\mathbf{b}_{I\alpha t} + \sum_{j=1}^{n_j}\sum_{I\in\mathcal{N}_j} N_I(\mathbf{x})J_j(\mathbf{x})\mathbf{c}_{Ij},\end{aligned} \tag{3a}$$

with

$$\{\boldsymbol{\Phi}_{\alpha t}(\mathbf{x})\}_{\alpha=1}^4 = \left\{\sqrt{r}\sin\frac{\theta}{2}, \sqrt{r}\cos\frac{\theta}{2}, \sqrt{r}\sin\theta\sin\frac{\theta}{2}, \sqrt{r}\sin\theta\cos\frac{\theta}{2}\right\}, \tag{3b}$$

where $\mathcal{N}$ is the set of all nodes in the mesh, $\mathcal{N}_c$ is the set of nodes whose shape function support is cut by the interior of the crack c, $\mathcal{N}_t$ is the set of nodes whose shape function support contains the crack-tip t and $\mathcal{N}_j$ is the set of nodes that are enriched for the junction j. In addition, $N_I(\mathbf{x})$ are the finite element shape functions, $H_c(\mathbf{x})$ is the generalized Heaviside function defined with respect to crack c, $\Phi_{\alpha t}(\mathbf{x})$ in (3b) are the crack-tip asymptotic functions defined with respect to crack-tip t (r and θ are the polar coordinates of a point in the coordinate system attached to the crack-tip), $J_j(\mathbf{x})$ is the junction function corresponding to the jth junction. The unknown coefficients of node I corresponding to the classical, Heaviside, near-tip and junction shape

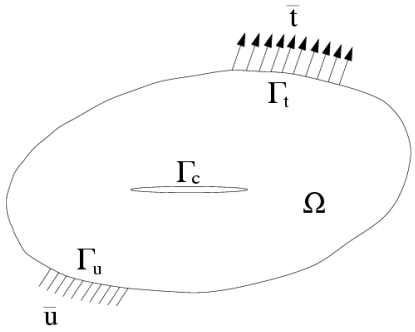

Figure 1. Boundary value problem with an internal traction-free crack.

functions are $\mathbf{u}_I$, $\mathbf{a}_{Ic}$, $\mathbf{b}_{I\alpha t}$ and $\mathbf{c}_{Ij}$, respectively. The number of cracks, crack-tips and junctions present in the domain are indicated by n_c, n_t and n_j, respectively.

In (3), multiple near-tip and junction enrichment functions are required in addition to the generalized Heaviside function to realize the correct displacement field to model the presence of a crack and its interactions with other existing cracks in the domain. On the other hand, with the harmonic enrichment functions that we use in this paper, the numerical enrichment function for a given crack is computed by considering its interactions with all other cracks in the domain. Thus, flexibility accrues and the complexity of the implementation is also significantly reduced. The extended finite element approximation for crack modeling with harmonic enrichment functions is:

$$\mathbf{u}^h(\mathbf{x}) = \sum_{I\in\mathcal{N}} N_I(\mathbf{x})\mathbf{u}_I + \sum_{c=1}^{n_c}\sum_{I\in\mathcal{N}_c} N_I(\mathbf{x})\psi_c(\mathbf{x})\mathbf{a}_{Ic}, \tag{4}$$

where $\psi_c(\mathbf{x})$ is the harmonic enrichment function of crack c. On substituting the trial and test approximations of the form (4) into (2), and using the arbitrariness of nodal variations, the discrete system of equations are obtained (see Reference [35]).

3. CONSTRUCTION OF HARMONIC ENRICHMENT FUNCTIONS

We now describe the algorithm for constructing harmonic enrichment functions through an illustrative crack problem. The aim, as proposed in Kaufmann et al. [10], is to calculate the enrichment function of a crack as the solution of the Laplace equation:

$$\Delta\psi_c(\mathbf{x}) = 0 \quad \text{in } \Omega_\ell, \tag{5a}$$

with Dirichlet and vanishing Neumann boundary conditions:

$$\psi_c = \pm 1 \quad \text{on } \Gamma_c^r, \quad \psi_c = 0 \quad \text{on } \partial\Gamma_c^r, \quad \nabla\psi_c \cdot \mathbf{n} = 0 \quad \text{on } \Gamma_\ell,\, \Gamma_d^r \quad (d = 1, 2, \ldots, n_c;\ d \neq c). \tag{5b}$$

The boundary-value problem posed in (5) is for the enrichment function of crack c with Γ_c^r denoting the rasterized crack path of crack c ($\partial\Gamma_c^r$ are the crack-tips), and $\Gamma_\ell \equiv \partial\Omega_\ell$ is the boundary of the Laplace domain. For a Laplace domain that is fully cut by a crack, the generalized Heaviside function satisfies the boundary-value problem in (5) and as a result the harmonic enrichment function $\psi_c(\mathbf{x})$ coincides with the generalized Heaviside function used in Moës et al. [2]. Furthermore, observe that the discontinuous crack-tip function, namely $\Phi_1(r, \theta) = \sqrt{r}\sin(\theta/2)$ in (3b), which is used in Belytschko and Black [1], is a harmonic function—solution of the mode III crack problem [36]. For a crack that terminates inside an element, the enrichment function Φ_1 can be recovered on using a sufficiently refined subgrid mesh and on imposing $\pm\sqrt{r}$ as the Dirichlet boundary conditions along the exact representation of the cracks [10]. However, it should be noted that the crack-tip function is recovered only sufficiently close to the crack. Away from the crack, the Neumann conditions have influence, and since the analytic crack-tip function does not satisfy the Neumann conditions, Φ_1 is not reproduced elsewhere. In light of the relatively coarse subgrid meshes we use and to keep the algorithm simple, we adopt the boundary conditions given in (5b). The use of the ± 1 Dirichlet

boundary conditions along the rasterized crack-path provides algorithmic simplicity without compromising accuracy in fracture computations (see Section 5).

Consider the computation of the enrichment function for crack 1 in a two-dimensional domain with two cracks (see Figure 2a). The domain is discretized with quadrilateral finite elements in Figure 2b. The nodes whose shape function support includes a crack-tip or is cut by a crack interior are enriched for that crack. This is similar to the standard X-FEM except that in our algorithm all the nodes that are enriched for a crack share one enrichment function and are treated similarly. The enriched nodes are marked with filled circles for crack 1 and open squares for crack 2 in Figure 2b. The Laplace domain is the set that contains all the elements that have at least one enriched node. For simplicity, we choose a rectangular box that contains all the enriched elements (the box in Figure 2b); however, the Laplace domain need not be rectangular and Kaufmann et al. [10] use a more compact domain. The Laplace domain is further refined into regular subgrid elements and the smooth crack paths are rasterized so that the cracks pass along the edges of the subgrid mesh (see Figure 2c). We demonstrate in Section 5 that the rasterized approximation of the crack paths does not adversely affect accuracy.

To model the discontinuity, all the nodes along the rasterized crack are duplicated and the connectivity of the subgrid elements are modified so that one copy of these nodes is connected to elements that lie above the crack and the other copy is connected to elements that are below the crack. This is similar to modeling a crack with conforming finite elements that allows the discontinuity to pass through the elements with the difference that herein the subgrid mesh is only used to compute the enrichment function. For crack 1, Dirichlet boundary conditions, namely $\psi = +1$ and $\psi = -1$ are assigned to the duplicated nodes above

and below the crack, respectively. A vanishing Neumann boundary condition, i.e., $\nabla\psi \cdot \mathbf{n} = 0$ is assigned to all the boundary nodes of the Laplace domain and also on the duplicated nodes along the rasterized path of crack 2. Once the Laplace equation is solved, bilinear finite element interpolation on the subgrid mesh is used to compute the enrichment function within the subgrid mesh. The numerical solution for the enrichment function of crack 1 is shown in Figure 2d. We remind the reader that the single numerical enrichment function that is obtained through the solution of (5) suffices for modeling crack 1, whereas in the standard X-FEM, generalized Heaviside function and multiple crack-tip enrichment functions are needed for the same purpose. The enrichment function of crack 2 is calculated similarly: Dirichlet boundary conditions are assigned along crack 2 with vanishing Neumann boundary conditions elsewhere. The enrichment function for crack 2 is depicted in Figure 2e. The same procedure is used in case of intersecting cracks with no additional overhead; in the standard X-FEM, an extra discontinuous enrichment must be added to the nodes containing the junction. Clearly, for two cracks that are sufficiently distant from each other, the effect of the vanishing Neumann boundary condition along one crack can be ignored when the harmonic enrichment function of the other crack is calculated. One can take advantage of this fact and choose a more compact Laplace domain containing only the cracks that are considered to be interacting with each other and as a result reduce the computational costs incurred in the Laplace solutions.

4. CONVERGENCE STUDY

We study the convergence properties of the X-FEM with harmonic enrichment function. Consider a plate defined over the region $(-1, 1) \times (-1, 1)$ with an edge crack starting from $(-1, 0)$ and ending at $(0, 0)$. The material of the plate is assumed to be homogeneous and

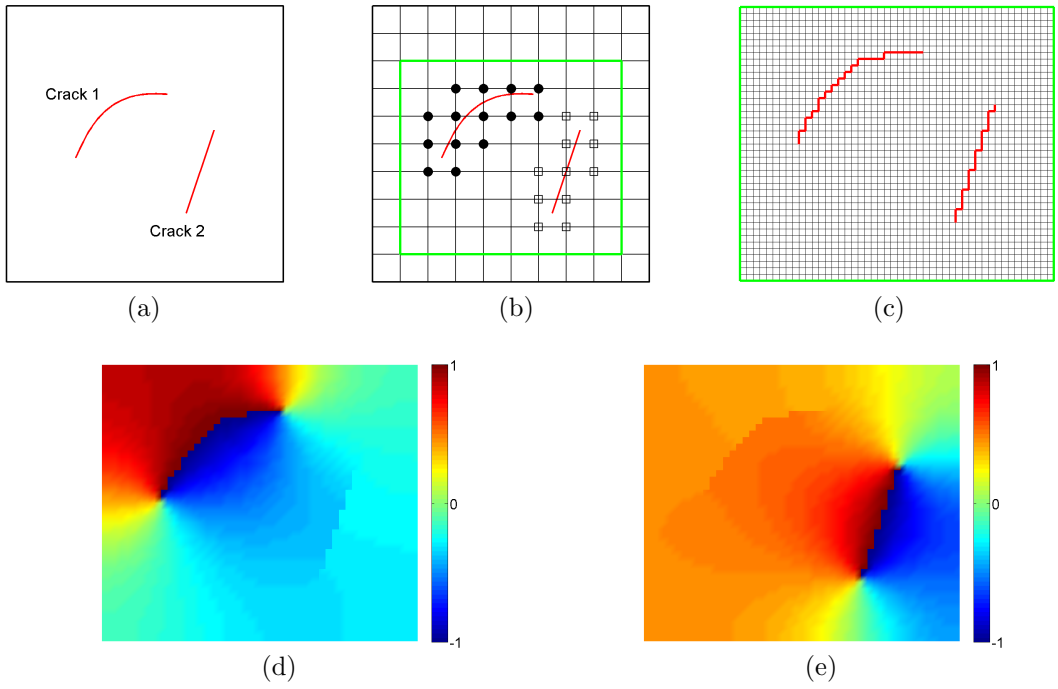

Figure 2. Algorithm for construction of harmonic enrichment functions. (a) geometry; (b) enriched nodes and Laplace domain; (c) subgrid mesh and *rasterized* approximation of the cracks (Manhattan paths); (d) enrichment function of crack 1; and (e) enrichment function of crack 2.

isotropic with the Young's modulus $E = 1$ and the Poisson ratio $\nu = 0$. The Cartesian components of mode I displacement field is used as the Dirichlet boundary conditions, which corresponds to $K_I = 1$ and $K_{II} = 0$. In order to realize the discontinuous Dirichlet boundary condition at $(-1, 0)$, two finite element nodes are placed at $(-1, \epsilon)$ and $(-1, -\epsilon)$, i.e., slightly above and below the crack, with ϵ a small positive number. The finite elements are connected to distinct nodes so that the exact displacement boundary condition can be imposed. This problem has been considered by Sukumar and Srolovitz [37] and Mousavi and Sukumar [29] to study the convergence of the X-FEM. We evaluate the relative energy norm of the error to

analyze the convergence of the harmonic X-FEM:

$$E_{rel} = \frac{||\mathbf{u} - \mathbf{u}^h||_{E(\Omega)}}{||\mathbf{u}||_{E(\Omega)}} = \frac{\left(\int_\Omega (\boldsymbol{\varepsilon} - \boldsymbol{\varepsilon}^h)^T \, \mathbf{C} \, (\boldsymbol{\varepsilon} - \boldsymbol{\varepsilon}^h) d\Omega\right)^{1/2}}{\left(\int_\Omega \boldsymbol{\varepsilon}^T \, \mathbf{C} \, \boldsymbol{\varepsilon} d\Omega\right)^{1/2}}, \tag{6}$$

where $\mathbf{u}$ and $\mathbf{u}^h$ are the exact and extended finite element solutions for the displacement field, $\boldsymbol{\varepsilon}$ and $\boldsymbol{\varepsilon}^h$ are the exact and extended finite element solutions for the strain tensor, and $\mathbf{C}$ is the constitutive matrix. First, we examine the convergence rate in the energy norm when only one layer of elements around the crack-tip are enriched (topological enrichment). Five different meshes are used: 10×10, 20×20, 40×40, 80×80 and 160×160. A sample mesh is shown in Figure 3a with the enriched nodes marked with filled squares. The convergence curves for 3×3 and 6×6 subgrid elements over each finite element are shown in Figure 3c—the rate of convergence is 0.500 and 0.499, respectively, which is in agreement with finite element theory for $\sqrt{r}$-singular problems. Also, it is seen from Figure 3c that refining the subgrid reduces the relative error but does not improve the convergence rate.

Next, we enrich a fixed area around the crack-tip as the mesh is refined (geometrical enrichment [31, 32], see Figure 3b). All the nodes within a distance of r_e from the crack-tip are enriched. Convergence curves for $r_e = 0.25$ and $r_e = 0.5$ are shown in Figure 3c. It is observed that the improvement in the accuracy and convergence rate is only marginal as the enrichment region is enlarged: convergence rate for 3×3 subgrid elements is 0.519 and 0.511 for $r_e = 0.25$ and $r_e = 0.5$, respectively, and for 6×6 subgrid elements is 0.524 and 0.513 for $r_e = 0.25$ and $r_e = 0.5$, respectively. While the X-FEM is capable of recovering the optimal convergence rate of unity in the energy norm via geometrical enrichment, the rate of convergence of harmonic X-FEM remains close to one-half. This is due to the fact that the harmonic enrichment function does not exactly reproduce the terms that are present in the asymptotic displacement field around the crack-tip, i.e., the analytical crack-tip functions that

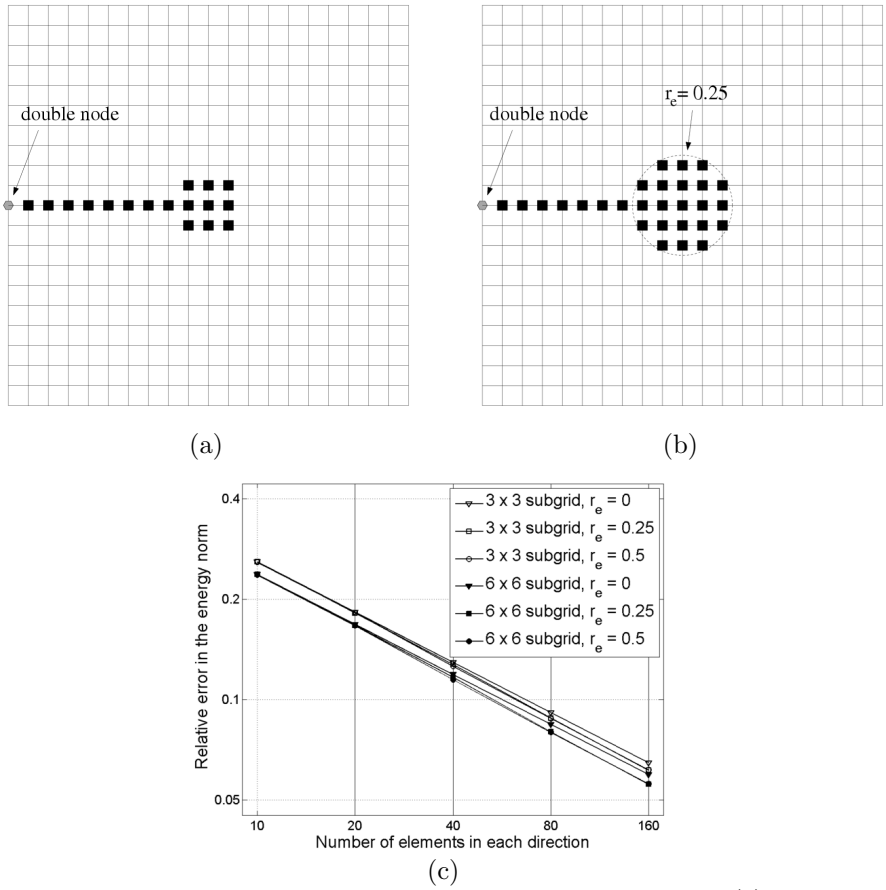

Figure 3. Convergence study of the X-FEM with harmonic enrichment. (a) enriched nodes for topological enrichment; (b) enriched nodes for geometrical enrichment ($r_e = 0.25$); and (c) relative energy norm of the error.

are used as the enrichment functions in the X-FEM.

5. NUMERICAL EXAMPLES

We present six benchmark crack problems to demonstrate the accuracy and effectiveness of the proposed enrichment scheme in fracture analyses with the X-FEM. Plane strain conditions are assumed, and the material is homogeneous and isotropic with Young's modulus $E = 1$ and Poisson's ratio $\nu = 0.3$. Four-node quadrilateral finite elements are used to discretize the domain for all the crack problems. A 2×2 Gauss quadrature rule is used in all elements that are not enriched. For each enriched element, numerical integration is done over the subgrid mesh; since the harmonic enrichment function is a bilinear polynomial, a 3×3 Gauss quadrature rule in each subgrid element provides exact integration for the stiffness matrix entries. Our numerical tests reveal that a 2×2 quadrature rule yields comparable accuracy to a 3×3 rule, and hence the former is preferred since it renders the numerical integration to be more efficient.

5.1. Edge-crack in a finite plate

First, we consider the benchmark problem of an edge-crack in a finite plate under tension. The geometry of the plate and crack configuration are shown in Figure 4a with $w = 7$, $h = 16$, $a/w = 1/2$, and $\sigma = 1$. The exact stress intensity factor (SIF) is: $K_I^* = 9.372$ [36]. The numerical enrichment function is obtained by solving the Laplace equation over a refined subgrid mesh around the crack as explained in Section 3.

The domain over which the Laplace equation is solved must contain all the elements that are enriched so that the enrichment function can be evaluated within all of them. In our implementation, the domain is chosen as the smallest rectangular box (see Figure 4b)

Table I. Normalized mode I stress intensity factor for the edge-crack problem.[a]

Mesh	X-FEM	Subgrid					
		2×2^b	3×3	4×4	6×6	8×8	16×16
21×41	0.954	0.933	0.902	0.942	0.946	0.949	0.951
41×81	0.977	0.961	0.945	0.966	0.968	0.970	0.971

[a] Reference solution: $K_I^* = 9.372$ [36].

[b] Each enriched finite element is divided into 2×2 subgrid elements.

that contains all the enriched elements. A contour plot of the enrichment function is shown in Figure 4c, in which the discontinuity is visible. The normalized mode I stress intensity factors that are computed using a standard implementation of the X-FEM and also with our numerical enrichment function are shown in Table I. For each mesh, the subgrid mesh for calculating the enrichment function is refined until the desired accuracy is obtained. In this case, a 6×6 subgrid mesh or finer over each finite element proves to be sufficient.

5.2. Inclined edge-crack in a finite plate

Consider the inclined edge-crack in a finite plate shown in Figure 5a with the dimensions $w = 1$ and $h = 2$, and under uniaxial tension $\sigma = 1$. The crack extends from $(0, 1)$ to $(0.4, 1.4)$. In Figure 5b, the enriched nodes are marked with filled circles and the Laplace domain is shown enclosed by a box. The enrichment function is depicted in Figure 5c. Mode I and mode II stress intensity factors for different finite element meshes and subgrid meshes are listed in Table II. The numerical results for the refined mesh are in good agreement with the reference solution provided in Sutradhar et al. [38].

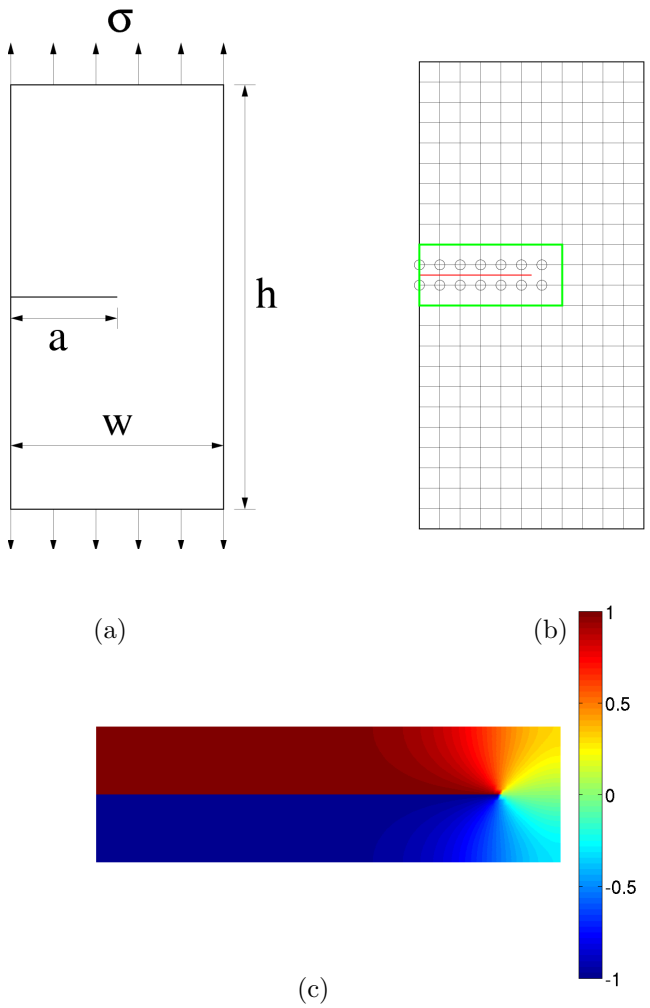

Figure 4. Edge-crack problem. (a) geometry; (b) enriched nodes and Laplace domain; and (c) enrichment function.

5.3. Inclined center-crack in an infinite plate

Consider an infinite plate with an inclined center-crack under biaxial loading (Figure 6a). The crack has a half-length of $a = 1/2$ and makes an angle of β with the vertical direction. The ratio $a/w = 1/10$ is selected so that the domain can accurately model an infinite plate. The tensile loads are chosen as $\sigma_1 = 1$ and $\sigma_2 = 2$. The normalized SIFs for different inclination

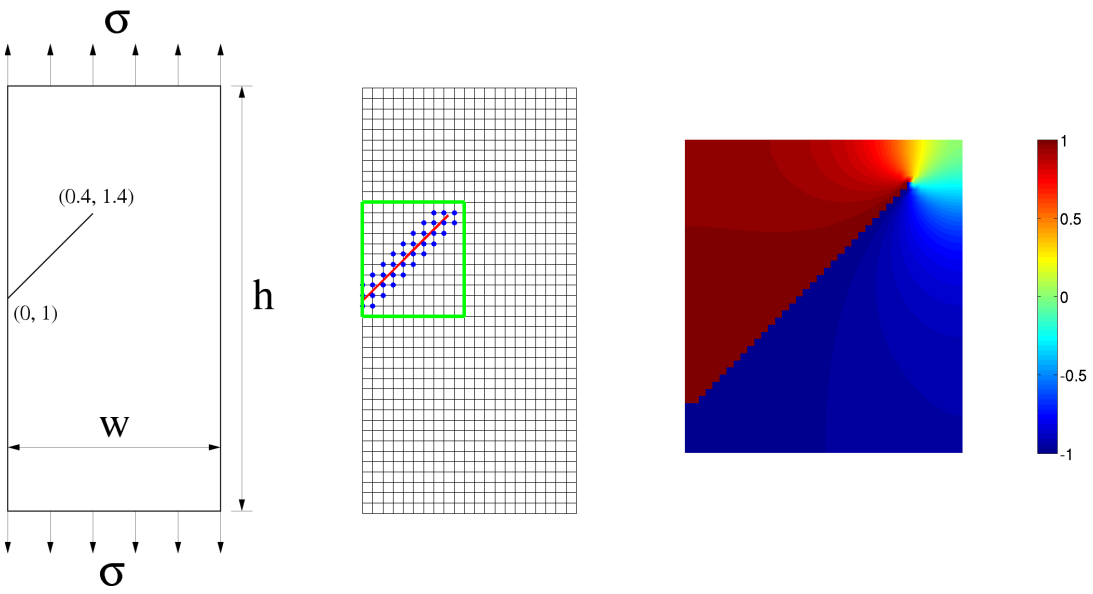

(a) (b) (c)

Figure 5. Inclined edge-crack problem. (a) geometry; (b) enriched nodes and Laplace domain; and (c) enrichment function.

Table II. Normalized stress intensity factors for the inclined edge-crack problem.[a]

SIFs	Mesh	X-FEM	Subgrid				
			2×2	3×3	4×4	6×6	8×8
K_I/K_I^*	21×41	0.979	0.874	0.938	0.900	0.942	0.947
	41×81	0.990	0.936	0.976	0.945	0.974	0.972
K_{II}/K_{II}^*	21×41	0.997	0.939	0.952	0.938	0.968	0.984
	41×81	0.998	0.949	0.984	0.950	0.988	0.990

[a] Reference solution: $K_I^* = 1.927$ and $K_{II}^* = 0.819$ [38].

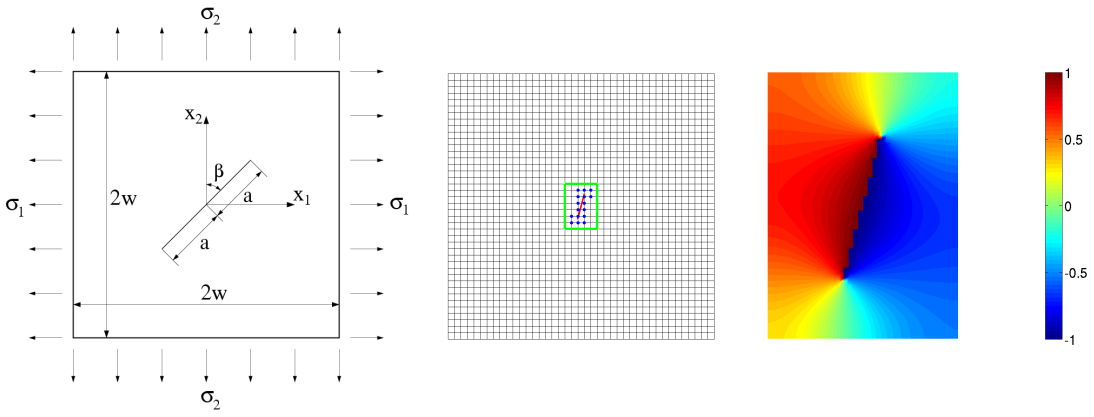

(a) (b) (c)

Figure 6. Inclined center-crack in an infinite plate. (a) geometry; (b) enriched nodes and Laplace domain; and (c) enrichment function.

Table III. Normalized stress intensity factors for an infinite plate with an inclined center crack (FE mesh: 41×41).

β	Exact [39]		X-FEM		Subgrid (3×3)		Subgrid (6×6)		Subgrid (10×10)	
	K_I^*	K_{II}^*	$\frac{K_I}{K_I^*}$	$\frac{K_{II}}{K_{II}^*}$	$\frac{K_I}{K_I^*}$	$\frac{K_{II}}{K_{II}^*}$	$\frac{K_I}{K_I^*}$	$\frac{K_{II}}{K_{II}^*}$	$\frac{K_I}{K_I^*}$	$\frac{K_{II}}{K_{II}^*}$
0	1.253	0.000	1.001	—	0.972	—	0.986	—	0.987	—
15	1.337	0.313	1.000	0.992	0.972	0.977	0.974	0.990	0.979	1.001
30	1.566	0.542	1.000	1.005	0.962	0.983	0.982	0.992	0.989	0.994
45	1.880	0.626	1.003	1.011	0.954	0.963	0.973	0.976	0.980	0.979
60	2.193	0.542	1.000	0.998	0.963	0.969	0.984	0.975	0.990	0.987
75	2.422	0.313	1.001	1.024	0.971	0.944	0.974	0.936	0.980	0.958
90	2.506	0.000	1.001	—	0.973	—	0.987	—	0.988	—

angles β and subgrid meshes are given in Table III, which are in good agreement with the exact solution of Aliabadi and Hall [39].

5.4. Intersecting cracks in a finite plate

To show the generality of the approach we use the numerical enrichment function to model a cross crack in a finite plate under unit biaxial loading (Figure 7a). The plate is a square of side length $w = 2$ and the crack half-length is $a = 1/2$. The crack is modeled as a main crack (AOB) with the enrichment function shown in Figure 7c and two branches (OD and OC) with their enrichment functions shown in Figures 7d and 7e, respectively. For the Laplace domain and enriched nodes, see Figure 7b: the nodes that are enriched for cracks AOB, OD and OC are marked with filled circles, open squares and asterisks, respectively. The nodes of the element containing the junction point are enriched for all the cracks. Normalized mode I stress intensity factor is computed at crack tips A and B and presented in Table IV. The numerical results are in excellent agreement with the reference solution provided in Cheung et al. [40].

Selecting the cracks as AOB, OD and OC ensures that the crack-opening and junction are appropriately represented—the calculated enrichment functions form a suitable basis for the enriched trial function space. However, it is not the only possible choice of basis functions and we show that there are other basis functions that can be used in the enriched space. For example, we choose AOC, OB and OD (see Figure 7a) as the cracks and apply the procedure outlined earlier to calculate the corresponding enrichment functions, which are now shown in Figures 7f, 7g and 7h. The SIFs calculated using these enrichment functions are presented in Table IV, and the numerical results obtained via the two different enrichment strategies are found to be of comparable accuracy.

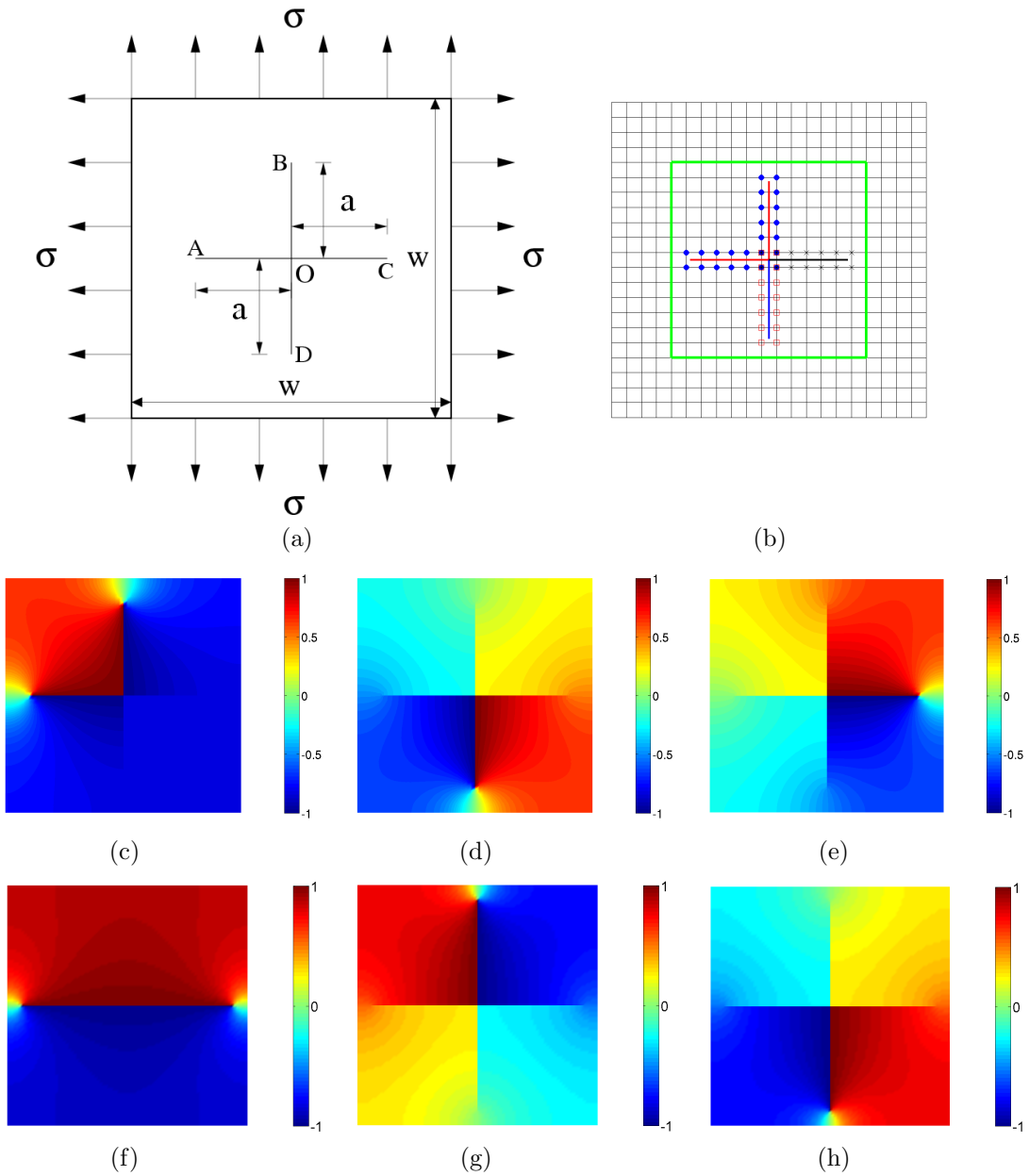

Figure 7. Intersecting cracks in a finite plate. (a) geometry; Crack combination AOB, OD and OC: (b) enriched nodes and Laplace domain; (c) enrichment function of crack AOB; (d) enrichment function of crack OD; and (e) enrichment function of crack OC. Crack combination AOC, OB and OD: (f) enrichment function of crack AOC; (g) enrichment function of crack OB; and (h) enrichment function of crack OD.

Table IV. Normalized stress intensity factors for cross-cracks in a finite plate.[a]

Crack combination	SIFs	Mesh	Subgrid	
			2×2	4×4
AOB, OC and OD	K_I^A/K_I^*	21×21	0.979	0.992
		41×41	0.993	0.999
	K_I^B/K_I^*	21×21	0.971	0.985
		41×41	0.985	0.993
AOC, OB and OD	K_I^A/K_I^*	21×21	0.963	0.978
		41×41	0.979	0.989
	K_I^B/K_I^*	21×21	0.996	1.006
		41×41	1.004	1.008

[a] Reference solution: $K_I^* = 1.281$ [40].

5.5. Branched crack in an infinite plate

We analyze a branched-crack (multiply-connected cracks) in an infinite plate under unit tensile loading (see Figure 8a). The plate has width $w = 40$ and height $h = 32$, and the crack is modeled as a main crack (AOC) and a branch (OB) with the dimensions $a = 1$, $b = 1$ and $\theta = \pi/4$. The Laplace domain is selected as the box containing all enriched elements as shown in Figure 8b. The enrichment function for each of the cracks is calculated by duplicating the nodes along both of the cracks and assigning Dirichlet boundary conditions along the corresponding crack only (Figures 8c and 8d) [10]. The normalized stress intensity factors for the tips A and B of the crack are listed in Table V for different finite element and subgrid meshes. The reference solutions are from Chen and Hasebe [41]. The extended finite element

Table V. Normalized stress intensity factors for the branched-crack problem.[a]

SIFs	Mesh	X-FEM [11]	Subgrid				
			2×2	3×3	4×4	6×6	8×8
K_I^A/K_I^{A*}	80×65	0.922[b]	0.913	0.948	0.952	0.967	0.974
	160×129	0.983[c]	0.953	0.950	0.978	0.985	0.982
K_I^B/K_I^{B*}	80×65	0.929[b]	1.079	1.060	1.038	1.015	1.031
	160×129	1.006[c]	1.048	0.933	1.007	0.996	1.006
K_{II}^B/K_{II}^{B*}	80×65	0.905[b]	1.048	1.100	1.024	1.015	1.008
	160×129	0.990[c]	1.016	0.795	0.998	0.993	1.008

[a] Reference solution: $K_I^{A*} = 1.709$, $K_I^{B*} = 0.810$, and $K_{II}^{B*} = 0.828$ [41].

[b] The element size parameter $h/a = 0.40$, where h is the average element size and a is shown in Figure 8a. In our implementation, the element size parameter for the mesh 80×65 is 0.5.

[c] The element size parameter $h/a = 0.22$. In our implementation, the element size parameter for the mesh 160×129 is 0.25.

solutions reported here are from Daux et al. [11] for the closest available element sizes. Our results are in good agreement with both the reference solutions and the X-FEM [11].

As shown in the previous example, other combinations of the cracks can also serve as the basis for the construction of the enrichment functions. The enrichment functions that are built by representing the cracks as AO and BOC are illustrated in Figures 8e and 8f. We obtain comparable results to those in Table V for this case too, but in the interest of space do not include these results.

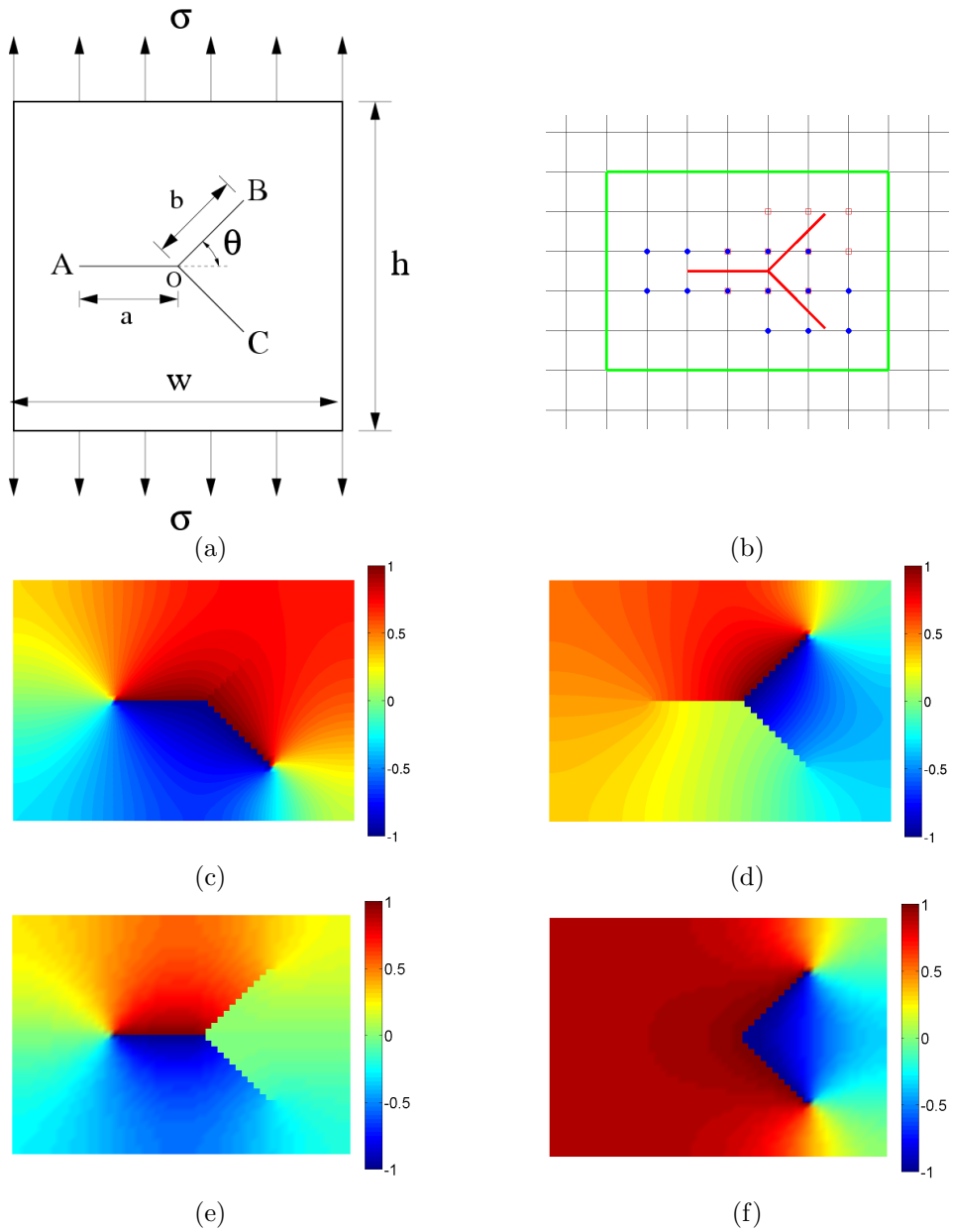

Figure 8. Branched-crack problem. (a) geometry; (b) enriched nodes and Laplace domain (zoom over the cracks); (c) enrichment function of crack AC; (d) enrichment function of crack OB; (e) enrichment function of crack AO; and (f) enrichment function of crack BC.

5.6. Arc-shaped crack in an infinite plate

As the last example, we consider the problem of an arc-shaped crack in an infinite plate to demonstrate that the rasterized approximation of the crack path in our algorithm does not limit its application to just straight cracks. In fact, it proves to be a convenient method to compute the enrichment function to model curved cracks, where otherwise the crack would be required to be approximated by many linear segments. The geometry of the plate, crack configuration and biaxial loading are shown in Figure 9a. The exact solution is [42]:

$$K_I = \frac{\sigma}{1+\sin^2\frac{\beta}{2}}\left[\frac{\pi R\sin\beta(1+\cos\beta)}{2}\right]^{1/2},\ K_{II} = \frac{\sigma}{1+\sin^2\frac{\beta}{2}}\left[\frac{\pi R\sin\beta(1-\cos\beta)}{2}\right]^{1/2}.$$

This problem was solved by Huang et al. [43] (bilinear finite elements) and Stazi et al. [44] (quadratic finite elements) using the X-FEM. To adequately represent the infinite domain, we choose the arc radius $R = 1$ within a plate of dimensions 20×20. To capture the curvature of the crack and to obtain accurate results, Huang et al. [43] used a structured mesh with Cartesian grid refinement in a narrow band near the crack. We adopt a similar approach and use two different element sizes: $h_e = 0.26$ is selected for elements far from the crack and $h_e = 0.02$ for the ones in the vicinity of the crack. A sample mesh with refinement in the region around the crack is shown in Figure 9b (enlarged image of the mesh near the crack appears in Figure 9c). Note that since the crack dimensions are much smaller than the problem domain, a sufficiently refined mesh is required in the vicinity of the crack. The enriched nodes and the Laplace domain of the crack is illustrated in Figure 9d for $\beta = 45^\circ$ and in Figure 9g for $\beta = 90^\circ$. The rasterized crack-path and the harmonic enrichment function for the arc-shaped crack is shown in Figures 9e and 9f for $\beta = 45^\circ$ and Figures 9h and 9i for $\beta = 90^\circ$, respectively. The normalized SIFs for different subgrid refinements are presented in Table VI, and we note that the numerical results are in good agreement with the exact solution [42]. This example

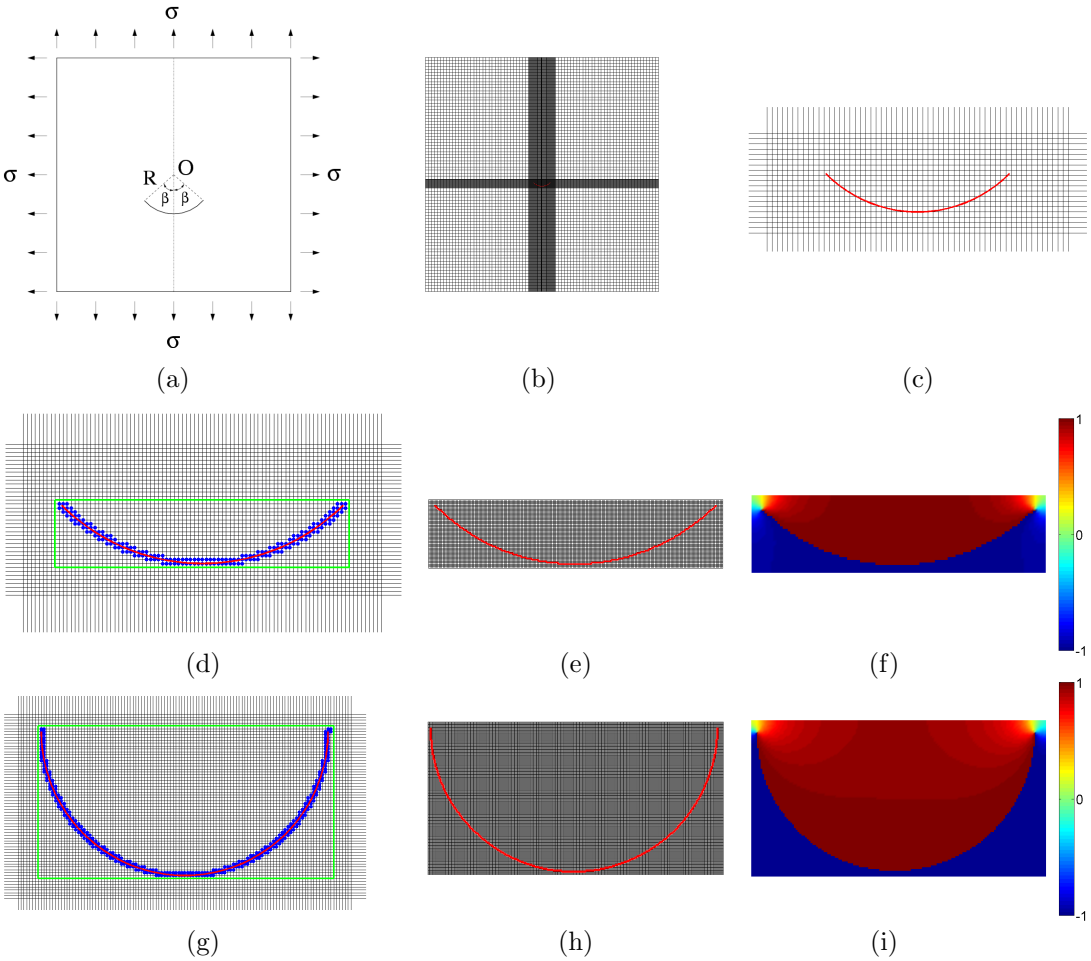

Figure 9. Arc-shaped crack in an infinite plate. (a) geometry; (b) sample mesh; (c) zoom over the Cartesian refinement of the mesh in the vicinity of the crack with the exact crack geometry; (d), (e) and (f) enriched nodes, Laplace domain, rasterized crack path and enrichment function for $\beta = 45°$, mesh parameters $[0.26, 0.02]$, and subgrid mesh of 3×3 over each element; and (g), (h) and (i) enriched nodes, Laplace domain, rasterized crack path and enrichment function for $\beta = 90°$, mesh parameters $[0.26, 0.02]$, and subgrid mesh of 3×3 over each element.

reveals that the harmonic enrichment function for a rasterized crack-path also yields accurate SIFs for a curved crack.

Table VI. Normalized stress intensity factors for the arc-shaped crack problem.[a]

β	Mesh parameters	SIFs	Subgrid		
			3×3	6×6	10×10
45°	$[0.26, 0.04]$	K_I/K_I^*	1.000	1.001	1.003
		K_{II}/K_{II}^*	0.913	0.949	0.962
	$[0.26, 0.02]$	K_I/K_I^*	1.001	1.001	1.001
		K_{II}/K_{II}^*	0.951	0.980	0.981
90°	$[0.26, 0.04]$	K_I/K_I^*	1.005	1.003	0.997
		K_{II}/K_{II}^*	0.985	0.986	0.964
	$[0.26, 0.02]$	K_I/K_I^*	0.999	0.999	0.999
		K_{II}/K_{II}^*	0.984	0.987	0.982

[a] Exact solution: $K_I^* = 1.201$ and $K_{II}^* = 0.497$ for $\beta = 45°$ and $K_I^* = K_{II}^* = 0.835$ for $\beta = 90°$ [42].

6. CONCLUDING REMARKS

We presented a unifying procedure to construct enrichment functions for crack modeling using the extended finite element method. The point of departure in this work was the numerical computation of the enrichment function via the solution of the Laplace equation with Dirichlet and vanishing Neumann boundary conditions. The Laplace domain was selected as the set that consisted of the union of all the elements with at least one enriched node and was discretized into a refined subgrid mesh. A rasterized approximation of the crack was used such that the crack passed along the boundaries of the subgrid elements but did not cut any of them. Regular four-node quadrilateral finite element meshes were used in the fracture computations.

Since there was no discontinuity inside a subgrid element and all basis functions (classical finite element and enriched) were piecewise polynomials, numerical integration with a standard 3×3 Gauss quadrature rule was exact; a 2×2 quadrature rule in subgrid elements proved to be sufficient for accurate numerical results.

A relative coarse uniform subgrid mesh (6×6 division of each enriched element) sufficed to realize acceptable accuracy in stress intensity factor computations. The generalization of the algorithm to branched cracks was straightforward: the branched crack was considered as a main crack and each branch was treated as a separate crack. In case of multiple and intersecting cracks, the enrichment function of each crack was calculated by setting Dirichlet boundary conditions along it and vanishing Neumann boundary conditions along all other cracks and the external boundary. This enrichment strategy took care of junctions automatically and there was no need to add extra discontinuous enrichment functions to the nodes whose shape function support contained the branching/intersecting point. Several benchmark numerical examples were presented that demonstrated the accuracy of the stress intensity factor computations and the robustness of the method in static fracture analyses. Good agreement with theory for the stress intensity factors was also realized for the problem of an arc-shaped crack, which further revealed the potential of the approach. The rate of convergence in energy norm for the X-FEM with harmonic enrichment functions was studied; a rate of one-half was realized, which matches the theoretical rate of the FEM for $\sqrt{r}$-singular problems. The convergence rate was only marginally improved when a fixed area was enriched. The numerically computed harmonic enrichment function deviates from the discontinuous asymptotic crack-tip function away from the crack-tip, and hence use of the fixed-area enrichment does not lead to an improvement in the convergence rate. Partitioning of the elements, which is required in

the standard implementation of the extended finite element method, is avoided, and exact integration is realized, albeit with the additional cost of numerical integration over a subgrid mesh. Harmonic enrichment functions provide an easy-to-implement and flexible approach for modeling multiple cracks, and intersecting and branched cracks in the extended finite element method.

ACKNOWLEDGEMENTS

S. E. Mousavi and N. Sukumar acknowledge the research support of the National Science Foundation through contract grants CMMI-0626481 and DMS-0811025 to the University of California at Davis. E. Grinspun is supported by the Sloan Foundation and the NSF (CAREER Award CCF-06-43268 and grants IIS-09-16129, IIS-05-28402, CNS-06-14770). The authors appreciate the helpful comments and suggestions of the anonymous reviewers, which led to the inclusion of the convergence study presented in Section 4.

REFERENCES

1. T. Belytschko and T. Black. Elastic crack growth in finite elements with minimal remeshing. *International Journal for Numerical Methods in Engineering*, 45(5):601–620, 1999.
2. N. Moës, J. Dolbow, and T. Belytschko. A finite element method for crack growth without remeshing. *International Journal for Numerical Methods in Engineering*, 46(1):131–150, 1999.
3. J. M. Melenk and I. Babuška. The partition of unity finite element method: Basic theory and applications. *Computer Methods in Applied Mechanics and Engineering*, 139:289–314, 1996.
4. I. Babuška and J. M. Melenk. The partition of unity method. *International Journal for Numerical Methods in Engineering*, 40:727–758, 1997.
5. G-H. Shi. Manifold method of material analysis. In *Transactions of the 9th Army Conference on Applied Mathematics and Computing*, pages 57–76, Minneapolis, Minnesota, 1991.

6. G. W. Ma, X. M. An, H. H. Zhang, and L. X. Li. Modeling complex crack problems using the numerical manifold method. *International Journal of Fracture*, 156:21–35, 2009.
7. G. W. Ma, X. M. An, and L. He. The numerical manifold method: A review. *International Journal of Computational Methods*, 7(1):1–32, 2010.
8. K. Terada, M. Asai, and M. Yamagishi. Finite cover method for linear and non-linear analyses of heterogeneous solids. *International Journal for Numerical Methods in Engineering*, 58:1321–1346, 2003.
9. A. Hansbo and P. Hansbo. A finite element method for the simulation of strong and weak discontinuities in solid mechanics. *Computer Methods in Applied Mechanics and Engineering*, 193(33–35):3523–3540, 2004.
10. P. Kaufmann, S. Martin, M. Botsch, E. Grinspun, and M. Gross. Enrichment textures for detailed cutting of shells. *ACM Transactions on Graphics*, 28(3):50:1–50:10, 2009.
11. C. Daux, N. Moës, J. Dolbow, N. Sukumar, and T. Belytschko. Arbitrary branched and intersecting cracks with the extended finite element method. *International Journal for Numerical Methods in Engineering*, 48(12):1741–1760, 2000.
12. T. Belytschko, N. Moës, S. Usui, and C. Parimi. Arbitrary discontinuities in finite elements. *International Journal for Numerical Methods in Engineering*, 50:993–1013, 2001.
13. A. Simone, C. A. Duarte, and E. Van der Giessen. A generalized finite element method for polycrystals with discontinuous grain boundaries. *International Journal for Numerical Methods in Engineering*, 67:1122–1145, 2006.
14. C. A. Duarte, L. G. Reno, and A. Simone. A high-order generalized FEM for through-the-thickness branched cracks. *International Journal for Numerical Methods in Engineering*, 72:325–351, 2007.
15. J. Dolbow, N. Moës, and T. Belytschko. Discontinuous enrichment in finite elements with a partition of unity method. *Finite Elements in Analysis and Design*, 36:235–260, 2000.
16. J. Dolbow, N. Moës, and T. Belytschko. Modeling fracture in Mindlin-Reissner plates with the extended finite element method. *International Journal of Solids and Structures*, 37:7161–7183, 2000.
17. N. Sukumar, Z. Y. Huang, J.-H. Prévost, and Z. Suo. Partition of unity enrichment for bimaterial interface cracks. *International Journal for Numerical Methods in Engineering*, 59(8):1075–1102, 2004.
18. A. Asadpoure and S. Mohammadi. Developing new enrichment functions for crack simulation in orthotropic media by the extended finite element method. *International Journal for Numerical Methods in Engineering*, 69:2150–2172, 2007.
19. E. Béchet, M. Scherzer, and M. Kuna. Application of the X-FEM to the fracture of piezoelectric materials.

International Journal for Numerical Methods in Engineering, 77:1535–1565, 2009.

20. N. Moës and T. Belytschko. Extended finite element method for cohesive crack growth. *Engineering Fracture Mechanics*, 69:813–833, 2002.
21. J. V. Cox. An extended finite element method with analytical enrichment for cohesive crack modeling. *International Journal for Numerical Methods in Engineering*, 78:48–83, 2008.
22. T. Elguedj, A. Gravouil, and A. Combescure. Appropriate extended functions for X-FEM simulation of plastic fracture mechanics. *Computer Methods in Applied Mechanics and Engineering*, 195:501–515, 2006.
23. T. Strouboulis, L. Zhang, and I. Babuška. Generalized finite element method using mesh-based handbooks: application to problems in domains with many voids. *Computer Methods in Applied Mechanics and Engineering*, 192:3109–3161, 2003.
24. T. Strouboulis, L. Zhang, and I. Babuška. p-version of the generalized FEM using mesh-based handbooks with applications to multiscale problems. *International Journal for Numerical Methods in Engineering*, 60:1639–1672, 2004.
25. C. A. Duarte and D.-J. Kim. Analysis and applications of a generalized finite element method with global-local enrichment functions. *Computer Methods in Applied Mechanics and Engineering*, 197:487–504, 2008.
26. G. Ventura. On the elimination of quadrature subcells for discontinuous functions in the extended finite-element method. *International Journal for Numerical Methods in Engineering*, 66:761–795, 2006.
27. D. J. Holdych, D. R. Noble, and R. B. Secor. Quadrature rules for triangular and tetrahedral elements with generalized functions. *International Journal for Numerical Methods in Engineering*, 73:1310–1327, 2008.
28. S. E. Mousavi, H. Xiao, and N. Sukumar. Generalized Gaussian quadrature rules on arbitrary polygons. *International Journal for Numerical Methods in Engineering*, 82:99–113, 2010.
29. S. E. Mousavi and N. Sukumar. Generalized Gaussian quadrature rules for discontinuities and crack singularities in the extended finite element method. *Computer Methods in Applied Mechanics and Engineering*, 2010. doi:10.1016/j.cma.2010.06.031.
30. T. Strouboulis, I. Babuška, and K. Copps. The design and analysis of the generalized finite element method. *Computer Methods in Applied Mechanics and Engineering*, 181(1–3):43–69, 2000.
31. E. Béchet, H. Minnebo, N. Moës, and B. Burgardt. Improved implementation and robustness study of the X-FEM for stress analysis around cracks. *International Journal for Numerical Methods in Engineering*, 64(8):1033–1056, 2005.

32. P. Laborde, J. Pommier, Y. Renard, and M. Salaün. High-order extended finite element method for cracked domains. *International Journal for Numerical Methods in Engineering*, 64:354–381, 2005.

33. S. E. Mousavi and N. Sukumar. Generalized Duffy transformation for integrating vertex singularities. *Computational Mechanics*, 45(2–3):127–140, 2010.

34. T. P. Fries and T. Belytschko. The extended/generalized finite element method: An overview of the method and its applications. *International Journal for Numerical Methods in Engineering*, 2010. DOI: 10.1002/nme.2914.

35. N. Sukumar and J.-H. Prévost. Modeling quasi-static crack growth with the extended finite element method. Part I: Computer implementation. *International Journal of Solids and Structures*, 40(26):7513–7537, 2003.

36. H. Ewalds and R. Wanhill. *Fracture Mechanics*. Edward Arnold, New York, 1989.

37. N. Sukumar and D. J. Srolovitz. Finite element-based model for crack propagation in polycrystalline materials. *Computational and Applied Mathematics*, 23:363–380, 2004.

38. A. Sutradhar, G. H. Paulino, and L. J. Gray. *Symmetric Galerkin Boundary Element Method*. Springer-Verlag, Berlin Heidelberg, 2008.

39. M. H. Aliabadi and W. S. Hall. Analytical removal of singularities and one-dimensional integration of three-dimensional boundary element method kernels. *Engineering Analysis with Boundary Elements*, 4:21–24, 1987.

40. Y. K. Cheung, C. W. Woo, and Y. H. Wang. A general method for multiple crack problems in a finite plate. *Computational Mechanics*, 10:335–343, 1992.

41. Y. Z. Chen and N. Hasebe. New integration scheme for the branch crack problem. *Engineering Fracture Mechanics*, 52(5):791–801, 1995.

42. G. C. Sih, P. C. Paris, and F. Erdogan. Crack-tip stress intensity factors for plane extension and plane bending problems. *Journal of Applied Mechanics*, 29:306–312, 1962.

43. R. Huang, N. Sukumar, and J.-H. Prévost. Modeling quasi-static crack growth with the extended finite element method. Part II: Numerical applications. *International Journal of Solids and Structures*, 40:7539–7552, 2003.

44. F. L. Stazi, E. Budyn, J. Chessa, and T. Belytschko. An extended finite element method with higher-order elements for curved cracks. *Computational Mechanics*, 31(1–2):38–48, 2003.

